ARPES studies of the inverse perovskite Ca_3PbO: Experimental confirmation of a candidate 3D Dirac fermion system

Yukiko Obata,[1] Ryu Yukawa,[2] Koji Horiba,[2] Hiroshi Kumigashira,[2] Yoshitake Toda,[3] Satoru Matsuishi,[3] and Hideo Hosono[1,3,*]

[1]*Laboratory for Materials and Structures, Institute of Innovative Research, Tokyo Institute of Technology, Yokohama 226-8503, Japan*

[2]*Photon Factory and Condensed Matter Research Center, Institute of Materials Structure Science, High Energy Accelerator Research Organization (KEK), Tsukuba 305-0801, Japan*

[3]*Materials Research Center for Element Strategy, Tokyo Institute of Technology, Yokohama 226-8503, Japan*

(Received 8 May 2017; published 9 October 2017)

We investigate the band structure of the inverse perovskite Ca_3PbO, a candidate three-dimensional (3D) Dirac fermion material, through soft x-ray angle-resolved photoemission spectroscopy. Conelike band dispersions are observed for Ca_3PbO, in close agreement with the predictions of electronic structure calculations. We further demonstrate that chemical substitution of Bi for Pb is effective in tuning the Fermi level of Ca_3PbO while leaving its electronic structure intact. Our study confirms that the inverse perovskite family provides a promising platform for the exploration of 3D Dirac fermion systems.

DOI: 10.1103/PhysRevB.96.155109

I. INTRODUCTION

Three-dimensional (3D) Dirac fermion systems have emerged as one of the most prominent topics in condensed matter physics. They comprise a class of topological materials in which bulk conduction and valence bands with linear energy-momentum dispersion relations meet at finite points or along curves in k space. These phenomena have been theoretically predicted and experimentally verified to occur at the phase transition point between a trivial insulator and a topological insulator [1–4], or in topological semimetals including those of the 3D Weyl [5–22], 3D Dirac [23–29], and topological nodal line semimetal (TNLS) [6,30–44] types.

Recently, there has been a growing interest in the cubic antiperovskite family as potential source of such novel topological phases of matter as 3D Z_2 invariant topological insulators [45], 3D massive Dirac fermions [46–48], topological crystalline insulators [49,50], TNLSs [34,35], and topological superconductors [51]. In particular, recent theoretical calculations on Ca_3PbO [46] [Fig. 1(a)], made of Ca^{2+}, Pb^{4-}, and O^{2-} ions, predict the presence of a 3D gapped Dirac-like cone at finite momentum along the Γ-X direction, which results from a band inversion of the Ca $3d$ and Pb $6p$ bands at the Γ point. Of paramount interest is the possibility that Ca_3PbO hosts 3D Dirac fermions with cubic symmetry as an intrinsic part of its electronic structure, since 3D Dirac fermions in other materials are sometimes only realized under such extreme conditions as low temperature or high pressure [52–54]. Like normal cubic perovskite materials, notably $SrVO_3$ [55], Ca_3PbO exhibits easy cleavage along (001) planes, which preserve a C_4 symmetry element in the bulk structure, a prerequisite for the protection of its bulk massive Dirac states and surface massless Dirac states. It is thus feasible to conduct experiments with a magnetic field applied along the C_4 rotation axis, as proposed previously [56]. Furthermore, the states near the Fermi level (E_F) are predicted to be derived entirely from Dirac-like bands with linear dispersion allowing for fundamental and direct studies of 3D Dirac fermions [46].

In order to verify the presence of 3D Dirac fermions experimentally, it is necessary to identify a Dirac point in 3D momentum space and investigate the electronic structure associated with the particular point not only along the surface-parallel directions (k_x or k_y) but also along the surface-perpendicular direction (k_z). These requirements call for an experimental probe with a good definition of k_z. Soft x-ray angle-resolved photoemission spectroscopy (SX-ARPES) is the most powerful method for directly studying the 3D electronic band structures of bulk materials, and has been demonstrated to provide a high-k_z resolution [57]. Thus, SX-ARPES using the tunable excitation energy of synchrotron radiation is eminently suited for the navigation of the 3D electronic structure of Ca_3PbO. In this paper we employ SX-ARPES to experimentally observe the Dirac-like band dispersion along the Γ-X direction in the 3D Brillouin zone (BZ) of bulk Ca_3PbO. By comparing these results with those for Bi-doped Ca_3PbO, we also show that electron doping leads to the shifts of the band structure downward, thereby demonstrating that aliovalent doping is effective in tuning the E_F of Ca_3PbO without fundamentally changing its Dirac-like band structure.

II. EXPERIMENT

As Ca_3PbO is reported to be highly air sensitive [58,59], the samples were prepared, handled, and stored in an Ar-filled glove box with residual oxygen and water levels below 1 ppm. First, polycrystalline Ca_3PbO was synthesized by solid-state reactions of CaO and Ca_2Pb. Both starting materials were weighed in a stoichiometric ratio, thoroughly mixed in a glass mortar, and heated at 950°C for 24 h. Next, the synthesized powder was combined with Ca metal as a flux in a molar ratio of 1:10 in an iron crucible and sealed in a stainless steel capsule. The capsule was heated up to 1000°C at a rate of 66.6°C/h and held at that temperature for 6 h. Subsequently, the temperature was slowly decreased to 800°C at a rate of 0.5°C/h and held there for 20 h. Finally, the crucible was taken out of the capsule and the residual Ca flux was removed by

*Corresponding author: hosono@msl.titech.ac.jp

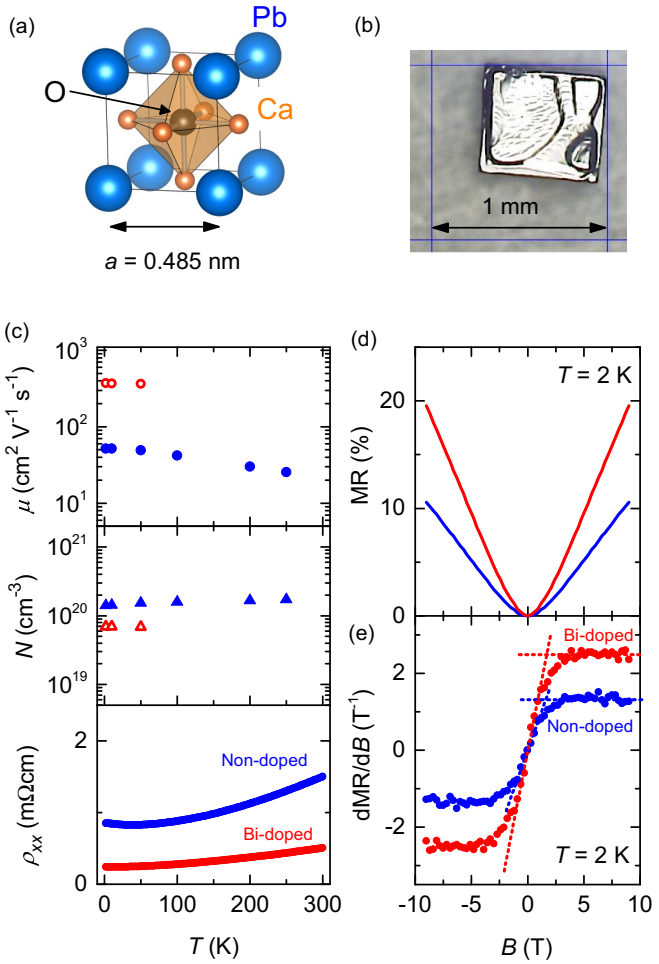

FIG. 1. The sample and the electron transport properties of Ca_3PbO. (a) The crystal structure of Ca_3PbO. (b) Photograph of a Ca_3PbO single crystal with clear squarelike facets. (c) Mobility, carrier density, and resistivity vs. temperature curves measured for Ca_3PbO and $Ca_3Pb_{0.92}Bi_{0.08}O$. (d), (e) Magnetoresistance (MR) and the first-order derivative of the MR with respect to magnetic field (B), dMR/dB, vs. B for Ca_3PbO and $Ca_3Pb_{0.92}Bi_{0.08}O$ at $T = 2$ K.

distillation at 800°C under vacuum. As a result, crystals with black color and squarelike facets [see Fig. 1(b)] were obtained. The size of the grown crystals reaches ∼1 mm, which is large enough to obtain well-cleaved sample surfaces for ARPES measurements. We also grew the electron-doped samples with a chemical formula $Ca_3(Pb_{1-x}Bi_x)O$ ($x = 0.07$). Synthesis of the Bi-doped single crystals followed the same procedure as that for the nondoped crystals, except that Ca_5Bi_3 was added as a Bi source to the Ca_2Pb and CaO starting materials, with the molar ratios being of the form $Ca_2Pb : Ca_5Bi_3 : CaO = 1 - x : 2x/5 : 1$.

Ca_3PbO crystallizes in a cubic inverse perovskite-type structure [Fig. 1(a)] with $a = 0.484$ nm and space group $Pm\bar{3}m$ [58]. The O atoms are located at the centers of the unit cell, surrounded by corner-sharing, regular Ca_6 octahedra. Single-crystal x-ray diffraction (SXRD) was performed on a 0.1 mm×0.1 mm×0.1 mm crystal using an R-AXIS RAPID II diffractometer and Mo K-alpha radiation, at room temperature. The crystals were mounted on a glass capillary. Afterward, to avoid exposure to air, they were immersed in liquid paraffin before transferring them from an Ar-filled glove box to the SXRD apparatus. Unit cell refinement was performed with CRYSTALCLEAR software (see Fig. S1(a) of Supplemental Material [60]). The samples were confirmed to have a cubic crystal structure with lattice parameter $a = 0.485(2)$ nm, matching that of polycrystalline Ca_3PbO.

The compositional formula of the nondoped single crystal used in the ARPES measurements was determined to be $Ca_{2.94(4)}Pb_{1.00(1)}O_{1.00(4)}$ by electron-probe microanalysis (EPMA), indicating that the crystals contain vacancies on 2% of the Ca sites. As for the Bi-doped samples, EPMA confirmed that the Bi content is almost comparable to the nominal value ∼0.07 and that the samples are also slightly Ca deficient.

Resistivity, Hall resistivity, and specific heat measurements were performed in the temperature range of 1.8–300 K and the magnetic field (B) range of −9 to 9 T using a physical property measurement system (Quantum Design). Cu wire contacts in the four-probe configuration were mounted to the sample with silver epoxy inside the Ar-filled glove box. The samples were heated in the glove box to 150°C to cure the epoxy. Samples were immersed in Paratone-N oil to prevent them from reacting with ambient air during the measurement. The electric current flowed in the ab plane while the applied B was parallel to the c axis.

In order to experimentally identify the 3D massive Dirac fermions, we performed bulk-sensitive SX-ARPES measurements at the beam line BL–2A MUSASHI at the Photon Factory, KEK. The tunable excitation energy of the synchrotron radiation source enabled us to trace the electronic structures in all three dimensions of momentum space. Samples were cleaved *in situ* at the measurement temperature of ∼20 K under an ultrahigh vacuum of 1×10^{-10} Torr, and the experimental data were collected using a Scienta SES-2002 electron energy analyzer with light linearly polarized along the horizontal direction. The energy and angular resolutions were set to approximately 170 meV and 0.3°, respectively.

To provide a theoretical reference with which to compare our ARPES results, we performed DFT band structure calculations with the Perdew-Burke-Ernzerhof (PBE) generalized-gradient approximation [61] using the VASP code [62], while the effective mass and hole carrier concentration were calculated using SKEAF code [63]. In agreement with the pioneering theoretical work on this compound [46], a Dirac electron is found to be located along the Γ-X direction in the BZ [Figs. 2(a) and 2(b)].

III. RESULTS AND DISCUSSION

A. Transport properties

Figure 1(c) shows the temperature dependence of the mobility, carrier density, and resistivity of the nondoped and the Bi-substituted Ca_3PbO samples. These measurements reveal metallic conduction with p-type carriers [see Fig. 1(c) and Fig. S1(b)]. Upon partially substituting Pb with Bi, the carrier density N slightly decreased from 1.4×10^{20} cm^{-3} to 6.9×10^{19} cm^{-3} at $T = 2$ K, but the Hall mobility μ significantly increased from 50 cm^2 V^{-1} s^{-1} to 370 cm^2 V^{-1} s^{-1} at this temperature [Fig. 1(c)]. The high hole carrier

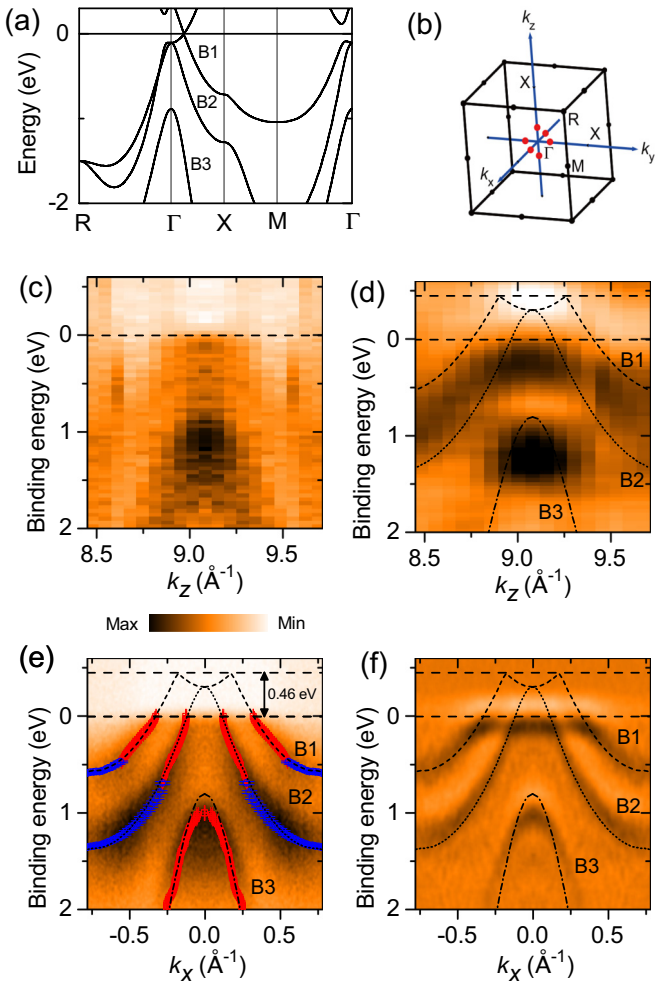

FIG. 2. Comparison of the measured and theoretically calculated band structures of Ca_3PbO. (a), (b) The PBE-DFT band structure of Ca_3PbO and its bulk BZ. Red dots highlight the six 3D Dirac point positions. (c), (e) ARPES intensity plots along the Γ-X lines of the k_z and k_x directions, respectively. The peak positions of the MDCs and EDCs are plotted by the red open squares and blue open circles, respectively. The intensity plots are symmetrized with respect to the center lines and averaged (see Fig. S3 of Supplemental Material [60]). Black dashed lines represent the results of band structure calculations. (d), (f), Second-derivative ARPES spectra along the Γ-X lines of the k_z and k_x directions, respectively.

concentration is consistent with the EPMA result indicating that both the nondoped and the Bi-substituted samples contain a Ca deficiency of 2%, which is likely to generate holes: $Ca_{Ca}^{\times} \rightarrow V_{Ca}'' + 2h^{\bullet} + Ca(g)$.

Figure 1(d) shows the magnetic-field (B) dependence of the magnetoresistance (MR) ratio for both nondoped and Bi-doped Ca_3PbO at $T = 2$ K, where the MR ratio (%) is defined as $[\rho(B)–\rho(0T)]/\rho(0T)\times 100$. The linear dependence of the MR ratio on the magnetic flux density B, one of the distinguishing magnetotransport properties of Dirac fermions [64], is clearly observed when the first-order derivative dMR/dB curve is investigated, as illustrated in Fig. 1(e). dMR/dB is semiclassically proportional to B^2 at low B, but it soon saturates at a critical field |B| of ∼1.6 T, which is defined as the point of intersection between the extrapolated slope at low B and the saturation level at high B (dotted lines). The linear B dependence observed at moderately low-B values in both nondoped and Bi-doped Ca_3PbO are characteristic features of Dirac fermions.

B. 3D nature of the band structure

The ARPES intensity image in Fig. 2(c) shows the band structure along the X-Γ-X path of the k_z axis, generated from ARPES scans at photon energies from 256–371 eV with the inner potential of 8.5 eV (see Supplemental Material [60]). The intensities in the binding energy range less than 1 eV are not sufficient to describe the band structure of Ca_3PbO near E_F. To better visualize the band structure, the second-derivative ARPES spectrum is illustrated in Fig. 2(d). The bands marked as B1 and B2 are still not so easy to distinguish for the k_z direction, showing that the Δk_z broadening (∼0.25 Å^{-1}) is too large to resolve these two bands that are also approximately 0.25 Å^{-1} apart from each other. In addition, the suppression of the intensity can be ascribed to matrix element effects. Despite the limit of resolution, it becomes possible to confirm the emergence of B1/B2 bands in the lower binding energy range and determine the photon energy of 311 eV corresponding to Γ in the 3D BZ. Through comparison with the PBE calculations, the band near the E_F is assigned to the Pb-6$p_{3/2}$ derived bands, while the band whose top reaches 1.0 eV is attributed to the Pb-6$p_{1/2}$ derived one. The Pb-6p band structure is consistent with the results of PBE calculations, though the E_F is shifted downward from the Dirac points.

Next, in order to see the band dispersion in more detail, we investigated the band structure of Ca_3PbO along the k_x direction, which provides equivalent information to that of Figs. 2(c) and 2(d) but with much higher momentum resolution. Figure 2(e) presents the resulting valence band structure along the X-Γ-X path of the k_x axis with $k_y = 0$ Å^{-1}, together with the plots of the peak positions of the momentum distribution curves (MDCs) and energy distribution curves (EDCs). The two Pb 6$p_{3/2}$ bands marked as B1 and B2 cross the E_F and consequently form hole pockets around the Γ point. The presence of these hole pockets is in accord with the results of transport measurements which revealed p-type conductivity.

C. Estimation of the Dirac point position and bandwidth

To elucidate the measured dispersions in detail, we compared the observed band dispersion near the E_F with that of the PBE calculations for the B1 band, which directly passes through the theoretical Dirac points (see Fig. S2(b) of the Supplemental Material [60]). To enable a quantitative discussion, the band dispersion of B1 determined by extracting the peak positions of the MDCs and EDCs along the Γ-X line is reproduced with a linear least-squares fit to the following phenomenological equation

$$E_{obs}(k_x) = E_{shift} + \alpha^* E_{cal}(k_x), \quad (1)$$

where E_{cal}, E_{shift} and α represent the calculated band dispersion, the energy shift, and the correction factor of the band mass m^*, respectively. Only E_{shift} and α are adjustable parameters

during the fit to the observed band dispersion. The best fit is obtained with $\alpha \sim 1.43(2)$ and $E_{\text{shift}} \sim 0.46(1)$ eV, showing that the bandwidth of the calculated B1 is expanded by 43% in our Ca_3PbO sample. By reducing the bandwidth of the experimental B1 by 1.43, the Dirac points originating from the B1 are estimated to reside 0.32(1) eV above the E_F. By assuming that the shape of actual band structure is similar to the calculated one, the hole concentration is estimated from the volume of Fermi surface obtained by calculated band structure with E_F shift of E_{shift}/α. The estimated concentration, 2.33×10^{20} cm^{-3} (B1: 2.07×10^{20} cm^{-3}, B2: 2.59×10^{19} cm^{-3}), almost agrees with the value $\sim1.4\times10^{20}$ cm^{-3} obtained from the Hall measurements. In addition, Fig. 2(e) shows that all the three Pb-6p bands are well reproduced by Eq. (1) with the same parameters, although there are some discrepancies at the energy positions near stationary points such as Γ. The agreement between the modified calculated bands and the APRES spectra is further confirmed by the matching between the second-derivative ARPES spectra and the modified PBE calculations in Fig. 2(f).

D. Bi-substitution effect on band structure

Next, in order to examine the effects of Bi substitution on the electronic structure of Ca_3PbO, we performed ARPES measurements on Bi-doped Ca_3PbO. Before the ARPES measurement, we measured the core-level spectra of the Bi-doped samples to check for a shift of the E_F due to Bi substitution (electron doping), as shown in Fig. 3(a). In comparing the peak positions of the Pb 4f between the nondoped and the Bi-doped Ca_3PbO samples, it becomes clear that Bi doping has induced a peak shift of ~0.12 eV toward higher binding energy, delineating the connection between Bi substitution and electron doping in Ca_3PbO.

Figure 3(c) illustrates the ARPES intensity plots for a Bi-doped crystal along the X-Γ-X path of the k_x direction at $k_y = 0$ Å^{-1} [cut A in Fig. 3(b)], overlaid with the plots of the peak positions of the MDCs and EDCs. The B1 band is similarly reproduced with a fit to Eq. (1) (see Fig. S2(c) of the Supplemental Material [60]). The best fit is obtained with $\alpha \sim 1.06(1)$ and $E_{\text{shift}} \sim 0.188(6)$ eV. By reducing the bandwidth of the experimental B1 by 1.06, the Dirac points are estimated to be located 0.176(6) eV above the E_F. Then, hole concentration is estimated to be 8.72×10^{19} cm^{-3} (B1: 8.21×10^{19} cm^{-3}, B2: 5.06×10^{18} cm^{-3}), relatively consistent with the value $\sim6.9\times10^{19}$ cm^{-3} obtained from Hall measurements. This result illustrates that the decrease in hole carrier concentration by Bi doping led to the decrease in the expansion of the bandwidth of the B1 from 43% to 6%. Although it is uncertain how the change in the bandwidth affects the massive Dirac states predicted in Ca_3PbO, it is evident that Bi doping contributes to the reformation of the bandwidth of the B1 to the theoretical one. The second-derivative ARPES spectra in Fig. 3(d) confirms the agreement between the experimental bands and modified calculated bands.

For a massive Dirac fermion, conelike band dispersions show finite curvature at the Dirac points. In Ca_3PbO, the Dirac fermion is predicted to be massive so that the corresponding band dispersions do not directly pass the Dirac point; therefore, their shape should become parabolic as the bands approach

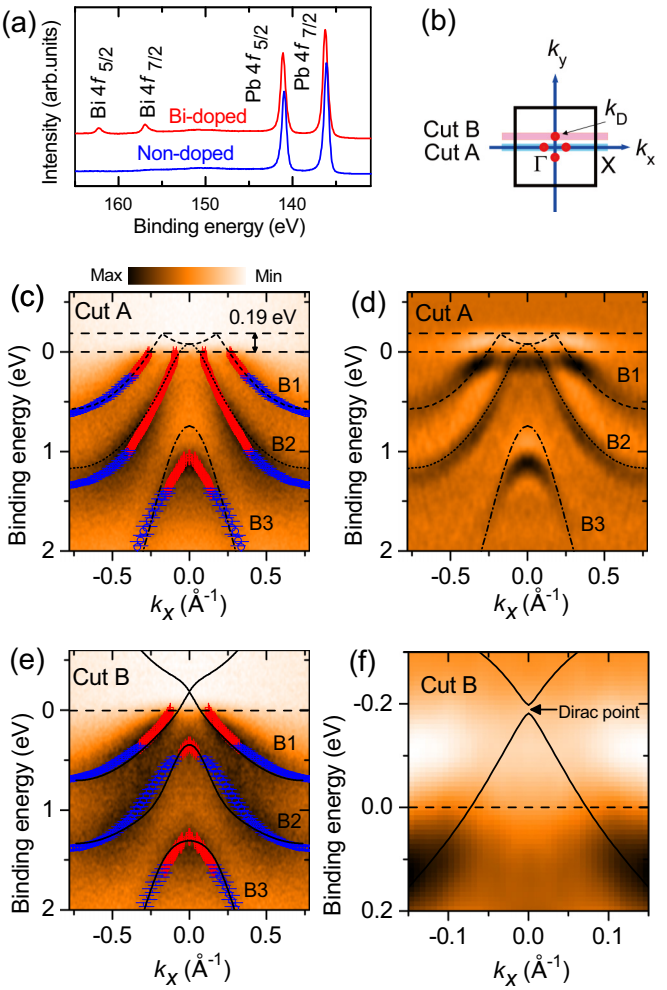

FIG. 3. (a) Core-level photoemission spectra of Ca_3PbO and $Ca_3Pb_{0.92}Bi_{0.08}O$. (b) 2D cross section of the BZ of Ca_3PbO. Red dots represent the four 3D Dirac points in the plane, denoted as k_D. (c), (e) ARPES intensity plots along cuts A and B, respectively, measured for a Bi-doped crystal. The peak positions of the MDCs and EDCs are plotted by the red open squares and blue open circles, respectively. (d), (f) Second-derivative ARPES spectra along cuts A and B, respectively. Black dashed and solid lines illustrate the results of band structure calculations for cut A and B, respectively.

the Dirac point, as verified in other massive Dirac fermion systems such as magnetically doped Bi_2Se_3 [65]. Figure 3(e) displays the ARPES intensity plots for measurements along cut B, which runs through a single Dirac point in Fig. 3(b), together with the results of the PBE calculations along cut B modified by using the parameters obtained in the fit of the B1 band along cut A to Eq. (1). The second-derivative ARPES spectra in Fig. 3(f) show some intensity above the E_F due to thermal excitation energy of $2k_BT$ (~3 meV). However, the intensity at ~0.01 eV above the E_F is attributed to some noise produced by taking the second derivative. In accord with the form of the calculated band structure, which becomes parabolic at the Dirac point as shown in Figs. 3(e) and 3(f), that of the experimental band structure is also relatively parabolic, consistent with the feature of the massive Dirac states.

IV. SUMMARY

We performed ARPES measurements on Ca_3PbO to examine whether or not it possesses 3D Dirac fermions. Our observations of the bulk Dirac-like band dispersions near E_F via SX-ARPES were consistent with the results of electronic structure calculations. This good agreement between calculated and experimental dispersion strongly supports that Ca_3PbO is host to native 3D Dirac fermions. In addition, we showed that the substitution of Bi for Pb in Ca_3PbO led to the reduction of the excess hole carrier concentration, the shift of the Dirac point relative to the E_F, and the reformation of the expanded bandwidth of the band comprising the Dirac point. Furthermore, we confirmed that Ca_3PbO can be cleaved along the (001) plane, which preserves the C_4 symmetry. These findings encourage further electron doping in Ca_3PbO to directly investigate the possibility of a finite mass gap in the Dirac-like band dispersions and the more extensive exploration of the inverse perovskite family as a promising venue for 3D Dirac fermion systems.

ACKNOWLEDGMENTS

We thank J. Yamaura, M. Kobayashi, M. Minohara, M. Kitamura, and T. Mitsuhashi for help with the SX-ARPES measurements at KEK-PF. Also, we thank Professor D. C. Fredrickson of University of Wisconsin for reading the manuscript. This work was supported by the Ministry of Education, Culture, Sports, Science and Technology Element Strategy Initiative to Form Core Research Center. The work at KEK-PF was performed under the approval of the Program Advisory Committee (Proposal 2016S2-004) at the Institute of Materials Structure Science, KEK.

[1] S. Murakami, New J. Phys. **9**, 356 (2007).
[2] S.-Y. Xu, Y. Xia, L. A. Wray, S. Jia, F. Meier, J. H. Dil, J. Osterwalder, B. Slomski, A. Bansil, H. Lin, R. J. Cava, and M. Z. Hasan, Science **332**, 560 (2011).
[3] T. Sato, K. Segawa, K. Kosaka, S. Souma, K. Nakayama, K. Eto, T. Minami, Y. Ando, and T. Takahashi, Nat. Phys. **7**, 840 (2011).
[4] J. Liu and D. Vanderbilt, Phys. Rev. B **90**, 155316 (2014).
[5] X. Wan, A. M. Turner, A. Vishwanath, and S. Y. Savrasov, Phys. Rev. B **83**, 205101 (2011).
[6] G. Xu, H. Weng, Z. Wang, X. Dai, and Z. Fang, Phys. Rev. Lett. **107**, 186806 (2011).
[7] M. Hirayama, R. Okugawa, S. Ishibashi, S. Murakami, and T. Miyake, Phys. Rev. Lett. **114**, 206401 (2015).
[8] Y. Sun, S.-C. Wu, M. N. Ali, C. Felser, and B. Yan, Phys. Rev. B **92**, 161107 (2015).
[9] A. A. Soluyanov, D. Gresch, Z. Wang, Q. Wu, M. Troyer, X. Dai, and B. A. Bernevig, Nature (London) **527**, 495 (2015).
[10] S.-M. Huang, S.-Y. Xu, I. Belopolski, C.-C. Lee, G. Chang, T.-R. Chang, B. Wang, N. Alidoust, G. Bian, M. Neupane, D. Sanchez, H. Zheng, H.-T. Jeng, A. Bansil, T. Neupert, H. Lin, and M. Z. Hasan, Proc. Natl. Acad. Sci. USA **113**, 1180 (2016).
[11] B. Q. Lv, H. M. Weng, B. B. Fu, X. P. Wang, H. Miao, J. Ma, P. Richard, X. C. Huang, L. X. Zhao, G. F. Chen, Z. Fang, X. Dai, T. Qian, and H. Ding, Phys. Rev. X **5**, 031013 (2015).
[12] S.-Y. Xu, I. Belopolski, N. Alidoust, M. Neupane, G. Bian, C. Zhang, R. Sankar, G. Chang, Z. Yuan, C.-C. Lee, S.-M. Huang, H. Zheng, J. Ma, D. S. Sanchez, B. Wang, A. Bansil, F. Chou, P. P. Shibayev, H. Lin, S. Jia, and M. Z. Hasan, Science **349**, 613 (2015).
[13] B. Q. Lv, N. Xu, H. M. Weng, J. Z. Ma, P. Richard, X. C. Huang, L. X. Zhao, G. F. Chen, C. E. Matt, F. Bisti, V. N. Strocov, J. Mesot, Z. Fang, X. Dai, T. Qian, M. Shi, and H. Ding, Nat. Phys. **11**, 724 (2015).
[14] L. X. Yang, Z. K. Liu, Y. Sun, H. Peng, H. F. Yang, T. Zhang, B. Zhou, Y. Zhang, Y. F. Guo, M. Rahn, D. Prabhakaran, Z. Hussain, S.-K. Mo, C. Felser, B. Yan, and Y. L. Chen, Nat. Phys. **11**, 728 (2015).
[15] S.-Y. Xu, N. Alidoust, I. Belopolski, Z. Yuan, G. Bian, T.-R. Chang, H. Zheng, V. N. Strocov, D. S. Sanchez, G. Chang, C. Zhang, D. Mou, Y. Wu, L. Huang, C.-C. Lee, S.-M. Huang, B. Wang, A. Bansil, H.-T. Jeng, T. Neupert, A. Kaminski, H. Lin, S. Jia, and M. Z. Hasan, Nat. Phys. **11**, 748 (2015).
[16] L. Huang, T. M. McCormick, M. Ochi, Z. Zhao, M.-T. Suzuki, R. Arita, Y. Wu, D. Mou, H. Cao, J. Yan, N. Trivedi, and A. Kaminski, Nat. Mater. **15**, 1155 (2016).
[17] K. Deng, G. Wan, P. Deng, K. Zhang, S. Ding, E. Wang, M. Yan, H. Huang, H. Zhang, Z. Xu, J. Denlinger, A. Fedorov, H. Yang, W. Duan, H. Yao, Y. Wu, S. Fan, H. Zhang, X. Chen, and S. Zhou, Nat. Phys. **12**, 1105 (2016).
[18] A. Tamai, Q. S. Wu, I. Cucchi, F. Y. Bruno, S. Riccò, T. K. Kim, M. Hoesch, C. Barreteau, E. Giannini, C. Besnard, A. A. Soluyanov, and F. Baumberger, Phys. Rev. X **6**, 031021 (2016).
[19] I. Belopolski, S.-Y. Xu, Y. Ishida, X. Pan, P. Yu, D. S. Sanchez, H. Zheng, M. Neupane, N. Alidoust, G. Chang, T.-R. Chang, Y. Wu, G. Bian, S.-M. Huang, C.-C. Lee, D. Mou, L. Huang, Y. Song, B. Wang, G. Wang, Y.-W. Yeh, N. Yao, J. E. Rault, P. Le Fèvre, F. Bertran, H.-T. Jeng, T. Kondo, A. Kaminski, H. Lin, Z. Liu, F. Song, S. Shin, and M. Z. Hasan, Phys. Rev. B **94**, 085127 (2016).
[20] F. Y. Bruno, A. Tamai, Q. S. Wu, I. Cucchi, C. Barreteau, A. de la Torre, S. McKeown Walker, S. Riccò, Z. Wang, T. K. Kim, M. Hoesch, M. Shi, N. C. Plumb, E. Giannini, A. A. Soluyanov, and F. Baumberger, Phys. Rev. B **94**, 121112(R) (2016).
[21] Y. Wu, D. Mou, N. H. Jo, K. Sun, L. Huang, S. L. Bud'ko, P. C. Canfield, and A. Kaminski, Phys. Rev. B **94**, 121113 (2016).
[22] C. Wang, Y. Zhang, J. Huang, S. Nie, G. Liu, A. Liang, Y. Zhang, B. Shen, J. Liu, C. Hu, Y. Ding, D. Liu, Y. Hu, S. He, L. Zhao, L. Yu, J. Hu, J. Wei, Z. Mao, Y. Shi, X. Jia, F. Zhang, S. Zhang, F. Yang, Z. Wang, Q. Peng, H. Weng, X. Dai, Z. Fang, Z. Xu, C. Chen, and X. J. Zhou, Phys. Rev. B **94**, 241119 (2016).
[23] Z. Wang, Y. Sun, X.-Q. Chen, C. Franchini, G. Xu, H. Weng, X. Dai, and Z. Fang, Phys. Rev. B **85**, 195320 (2012).
[24] Z. K. Liu, B. Zhou, Y. Zhang, Z. J. Wang, H. M. Weng, D. Prabhakaran, S.-K. Mo, Z. X. Shen, Z. Fang, X. Dai, Z. Hussain, and Y. L. Chen, Science **343**, 864 (2014).

[25] S.-Y. Xu, C. Liu, S. K. Kushwaha, R. Sankar, J. W. Krizan, I. Belopolski, M. Neupane, G. Bian, N. Alidoust, T.-R. Chang, H.-T. Jeng, C.-Y. Huang, W.-F. Tsai, H. Lin, P. P. Shibayev, F.-C. Chou, R. J. Cava, and M. Z. Hasan, Science **347**, 294 (2015).
[26] Z. Wang, H. Weng, Q. Wu, X. Dai, and Z. Fang, Phys. Rev. B **88**, 125427 (2013).
[27] Z. K. Liu, J. Jiang, B. Zhou, Z. J. Wang, Y. Zhang, H. M. Weng, D. Prabhakaran, S.-K. Mo, H. Peng, P. Dudin, T. Kim, M. Hoesch, Z. Fang, X. Dai, Z. X. Shen, D. L. Feng, Z. Hussain, and Y. L. Chen, Nat. Mater. **13**, 677 (2014).
[28] M. Neupane, S.-Y. Xu, R. Sankar, N. Alidoust, G. Bian, C. Liu, I. Belopolski, T.-R. Chang, H.-T. Jeng, H. Lin, A. Bansil, F. Chou, and M. Z. Hasan, Nat. Commun. **5**, 3786 (2014).
[29] S. Borisenko, Q. Gibson, D. Evtushinsky, V. Zabolotnyy, B. Büchner, and R. J. Cava, Phys. Rev. Lett. **113**, 027603 (2014).
[30] K. Mullen, B. Uchoa, and D. T. Glatzhofer, Phys. Rev. Lett. **115**, 026403 (2015).
[31] C. Fang, Y. Chen, H.-Y. Kee, and L. Fu, Phys. Rev. B **92**, 081201 (2015).
[32] Y. Chen, Y. Xie, S. A. Yang, H. Pan, F. Zhang, M. L. Cohen, and S. Zhang, Nano Lett. **15**, 6974 (2015).
[33] H. Weng, Y. Liang, Q. Xu, R. Yu, Z. Fang, X. Dai, and Y. Kawazoe, Phys. Rev. B **92**, 045108 (2015).
[34] Y. Kim, B. J. Wieder, C. L. Kane, and A. M. Rappe, Phys. Rev. Lett. **115**, 036806 (2015).
[35] R. Yu, H. Weng, Z. Fang, X. Dai, and X. Hu, Phys. Rev. Lett. **115**, 036807 (2015).
[36] L. S. Xie, L. M. Schoop, E. M. Seibel, Q. D. Gibson, W. Xie, and R. J. Cava, APL Mater. **3**, 083602 (2015).
[37] Y.-H. Chan, C.-K. Chiu, M. Y. Chou, and A. P. Schnyder, Phys. Rev. B **93**, 205132 (2016).
[38] M. Zeng, C. Fang, G. Chang, Y.-A. Chen, T. Hsieh, A. Bansil, H. Lin, and L. Fu, arXiv:1504.03492 (2015).
[39] A. Yamakage, Y. Yamakawa, Y. Tanaka, and Y. Okamoto, J. Phys. Soc. Jpn. **85**, 013708 (2015).
[40] J. Zhao, R. Yu, H. Weng, and Z. Fang, Phys. Rev. B **94**, 195104 (2016).
[41] G. Bian, T.-R. Chang, H. Zheng, S. Velury, S.-Y. Xu, T. Neupert, C.-K. Chiu, S.-M. Huang, D. S. Sanchez, I. Belopolski, N. Alidoust, P.-J. Chen, G. Chang, A. Bansil, H.-T. Jeng, H. Lin, and M. Z. Hasan, Phys. Rev. B **93**, 121113 (2016).
[42] M. Hirayama, R. Okugawa, T. Miyake, and S. Murakami, Nat. Commun. **8**, 14022 (2017).
[43] G. Bian, T.-R. Chang, R. Sankar, S.-Y. Xu, H. Zheng, T. Neupert, C.-K. Chiu, S.-M. Huang, G. Chang, I. Belopolski, D. S. Sanchez, M. Neupane, N. Alidoust, C. Liu, B. Wang, C.-C. Lee, H.-T. Jeng, C. Zhang, Z. Yuan, S. Jia, A. Bansil, F. Chou, H. Lin, and M. Z. Hasan, Nat. Commun. **7**, 10556 (2016).
[44] Y. Wu, L.-L. Wang, E. Mun, D. D. Johnson, D. Mou, L. Huang, Y. Lee, S. L. Bud'ko, P. C. Canfield, and A. Kaminski, Nat. Phys. **12**, 667 (2016).
[45] Y. Sun, X.-Q. Chen, S. Yunoki, D. Li, and Y. Li, Phys. Rev. Lett. **105**, 216406 (2010).
[46] T. Kariyado and M. Ogata, J. Phys. Soc. Jpn. **81**, 064701 (2012).
[47] D. Samal, H. Nakamura, and H. Takagi, APL Mater. **4**, 076101 (2016).
[48] Y. Okamoto, A. Sakamaki, and K. Takenaka, J. Appl. Phys. **119**, 205106 (2016).
[49] T. H. Hsieh, J. Liu, and L. Fu, Phys. Rev. B **90**, 081112 (2014).
[50] C.-K. Chiu, Y.-H. Chan, X. Li, Y. Nohara, and A. P. Schnyder, Phys. Rev. B **95**, 035151 (2017).
[51] M. Oudah, A. Ikeda, J. N. Hausmann, S. Yonezawa, T. Fukumoto, S. Kobayashi, M. Sato, and Y. Maeno, Nat. Commun. **7**, 13617 (2016).
[52] P. Dziawa, B. J. Kowalski, K. Dybko, R. Buczko, A. Szczerbakow, M. Szot, E. Łusakowska, T. Balasubramanian, B. M. Wojek, M. H. Berntsen, O. Tjernberg, and T. Story, Nat. Mater. **11**, 1023 (2012).
[53] T. Liang, Q. Gibson, J. Xiong, M. Hirschberger, S. P. Koduvayur, R. J. Cava, and N. P. Ong, Nat. Commun. **4**, 2696 (2013).
[54] X. Xi, X.-G. He, F. Guan, Z. Liu, R. D. Zhong, J. A. Schneeloch, T. S. Liu, G. D. Gu, X. Du, Z. Chen, X. G. Hong, W. Ku, and G. L. Carr, Phys. Rev. Lett. **113**, 096401 (2014).
[55] T. Yoshida, K. Tanaka, H. Yagi, A. Ino, H. Eisaki, A. Fujimori, and Z.-X. Shen, Phys. Rev. Lett. **95**, 146404 (2005).
[56] H. B. Nielsen and M. Ninomiya, Phys. Lett. B **130**, 389 (1983).
[57] V. N. Strocov, M. Shi, M. Kobayashi, C. Monney, X. Wang, J. Krempasky, T. Schmitt, L. Patthey, H. Berger, and P. Blaha, Phys. Rev. Lett. **109**, 086401 (2012).
[58] A. Widera and H. Schäfer, Mater. Res. Bull. **15**, 1805 (1980).
[59] J. Nuss, C. Mühle, K. Hayama, V. Abdolazimi, and H. Takagi, Acta Crystallogr. Sect. B Struct. Sci. Cryst. Eng. Mater. **71**, 300 (2015).
[60] See Supplemental Material at http://link.aps.org/supplemental/10.1103/PhysRevB.96.155109 for details on sample characterization and ARPES data analysis.
[61] J. P. Perdew, K. Burke, and M. Ernzerhof, Phys. Rev. Lett. **77**, 3865 (1996).
[62] G. Kresse and J. Hafner, Phys. Rev. B **47**, 558 (1993).
[63] P. M. C. Rourke and S. R. Julian, Comput. Phys. Commun. **183**, 324 (2012).
[64] A. A. Abrikosov, Phys. Rev. B **58**, 2788 (1998).
[65] Y. L. Chen, J.-H. Chu, J. G. Analytis, Z. K. Liu, K. Igarashi, H.-H. Kuo, X. L. Qi, S. K. Mo, R. G. Moore, D. H. Lu, M. Hashimoto, T. Sasagawa, S. C. Zhang, I. R. Fisher, Z. Hussain, and Z. X. Shen, Science **329**, 659 (2010).